# Dissociation of Intestinal and Hepatic Activities of FXR and LXRα Supports Metabolic Effects of Terminal Ileum Interposition in Rodents

Andrea Mencarelli,[1] Barbara Renga,[1] Claudio D'Amore,[1] Chiara Santorelli,[2] Luigina Graziosi,[2] Angela Bruno,[1] Maria Chiara Monti,[3] Eleonora Distrutti,[4] Sabrina Cipriani,[1] Annibale Donini,[2] and Stefano Fiorucci[1]

The farnesoid X receptor (FXR) and the liver x receptors (LXRs) are bile acid–activated receptors that are highly expressed in the enterohepatic tissues. The mechanisms that support the beneficial effects of bariatric surgery are only partially defined. We have investigated the effects of ileal interposition (IT), a surgical relocation of the distal ileum into the proximal jejunum, on FXR and LXRs in rats. Seven months after surgery, blood concentrations of total bile acids, taurocholic acid, an FXR ligand, and taurohyocholic acid, an LXRα ligand, were significantly increased by IT ($P < 0.05$). In contrast, liver and intestinal concentrations of conjugated and nonconjugated bile acids were decreased ($P < 0.05$). These changes were associated with a robust induction of FXR and FXR-regulated genes in the intestine, including Fgf15, a negative regulator of bile acid synthesis. IT repressed the liver expression of glucose-6-phosphatase (G6PC) and phosphoenolpyruvate carboxykinase (Pepck), two gluconeogenetic genes, along with the expression of LXRα and its target genes sterol regulatory element-binding protein (Srebp) 1c and fatty acid synthase (Fas) in the liver. Treating IT rats with chenodeoxycholic acid ameliorated insulin signaling in the liver. Whether confirmed in human settings, these results support the association of pharmacological therapies with bariatric surgeries to exploit the selective activation of intestinal nuclear receptors. ***Diabetes*** **62:3384–3393, 2013**

**T**he farnesoid receptor (FXR) and liver X receptors (LXRs) are members of the nuclear receptor superfamily of transcription factors activated by bile acids and oxysterols (1,2). FXR, the master regulator of bile acid metabolism, is expressed mainly in the liver, intestine, kidney, and adrenal glands (1,2). In the liver, FXR engages a feedback loop that inhibits bile acid synthesis through induction of small heterodimer partner (SHP). SHP interacts with liver receptor homolog 1 (LRH1) to form a heterodimer, resulting in the repression of cytochrome P450 7A1 (CYP7A1), the rate-limiting enzyme in the conversion of cholesterol to bile acids (3,4). In the

intestine, FXR inhibits the absorption of bile salts through modulation of several transport proteins. FXR-dependent downregulation of the apical sodium-dependent bile salt transporter (IBAT) is believed to be mediated through SHP-dependent inhibition of LRH1 (5). In addition, FXR promotes transport of bile salts from the apical to the basolateral membrane of enterocytes through the up-regulation of ileal bile acid-binding protein (IBABP) (6). Bile acids are then released into the portal circulation for return to the liver through FXR-induced expression of the organic solute transporters OSTα and OSTβ (7). Finally, FXR is a negative modulator of the sodium taurocholate cotransporting polypeptide (NTCP), which mediates absorption of bile acids from the portal circulation, thus limiting hepatic bile salt levels (8). Another important function of FXR is the reduction of lipogenic pathways though downregulation of sterol regulatory element-binding protein 1C (SREBP1C) and fatty acid synthase (FAS) genes (8). In addition, FXR plays a substantial role in regulating hepatic carbohydrate metabolism (9). Indeed, FXR activation exerts differential effects on the regulation of hepatic gluconeogenesis during the transition from the fasting to the fed state in mice. Thus, although the pharmacological activation of FXR in fed conditions negatively regulates gluconeogenic genes phosphoenolpyruvate carboxykinase (PEPCK) and glucose-6-phosphatase (G6PC) in the liver, its activation in fasting does the opposite (9,10), partially explaining why FXR deficiency in rodent models of obesity seems to have a beneficial impact on both body weight and glucose homeostasis (11). In contrast to the liver, activation of intestinal FXR exerts beneficial effects on glucose homeostasis. Thus, the activation of intestinal FXR in the murine distal ileum induces the release of fibroblast growth factor 15 (*Fgf15*) (FGF19 is the human ortholog), a hormone that once secreted in the portal circulation, reaches the liver to bind to the fibroblast growth factor receptor (FGFR) 4, repressing bile acid synthesis and the expression of gluconeogenic genes (12–14). This mechanism facilitates a crosstalk between the intestine and liver for the regulation of hepatic glucose production and is an appealing pharmacological target.

LXRs are ligand-activated nuclear receptors that act as cholesterol sensors. LXRα is expressed in tissues with a high metabolic activity, including liver, adipose, and macrophages, whereas LXRβ is ubiquitously expressed (1). Both LXRs are activated by cholesterol derivatives, including oxysterols and 24(S),25-epoxycholesterol. Moreover, LXRs are activated by bile acids, such as hyocholic acid (HCA) and hyodeoxycholic acid (HDCA) (1,2). One of the best-characterized effects of LXRα is to promote

reverse cholesterol transport (RCT), the process of cholesterol delivery from the periphery to the liver for excretion. The first step in RCT is the transfer of cholesterol to lipid-poor molecules in the plasma, such as apolipoprotein A1 and pre-β HDL through ATP-binding cassette transporter A1 (ABCA1). LXRα agonists induce ABCA1 expression in an LXR-dependent manner in macrophages and intestine (15). Another major function of LXRα in the intestine is the induction of the transporters ABCG5 and ABCG8, which heterodimerize into a complex that mediates the apical efflux of cholesterol from enterocytes (16). In rodents but not in humans, LXRα activation enhances hepatic cholesterol catabolism partly through increased expression of CYP7A1, which is the rate-limiting enzyme in the classical conversion of cholesterol to bile acids (17). Other LXR target genes are SREBP1C and FAS (18–20), which promote de novo lipogenesis, and CD36, a membrane receptor capable of uptaking modified forms of LDLs and fatty acids from the circulation (21).

Bariatric surgery is attracting increasing consideration for its role in the treatment of morbid obesity and type 2 diabetes (22). Despite several treatment modalities that have been developed, the mechanisms that support the beneficial effects of different surgical approaches are only partially defined. In the current study, we provide evidence that ileal interposition (IT) leads to a selective activation of the intestinal nuclear receptors FXR and LXRα while repressing the expression/activity of these ligand-activated transcription factors in rat liver. Because in ileal-transposed animals hepatic FXR and LXRα become resistant to pharmacological activation, the findings provide a molecular explanation to the metabolic effects of bariatric surgery on glucose and lipid homeostasis and ground the basis for pharmacological exploitation of intestinal FXR and LXRα in the treatment of type 2 diabetes and obesity in patients undergoing bariatric surgery.

## RESEARCH DESIGN AND METHODS

**Animal models.** Male Wistar rats (300–325 g) were purchased from Harlan Italy (San Pietro al Natisone, Italy). Rats were housed under controlled temperature (22°C) and photoperiods (12:12-h light/dark cycle) and allowed unrestricted access to standard rat chow and tap water. All animal experimental procedures were approved by the Ethics Committee of the University of Perugia and by the Italian Health Ministry. The IT surgery involved the removal and repositioning of a distal ileum segment to the proximal jejunum in a pro peristaltic direction, taking care to maintain the continuity of the gastrointestinal tract and to preserve neurovascular connections. Rats undergoing surgery were fasted overnight, anesthetized with gaseous anesthesia (2% isoflurane), and placed on a warm platform. A small midline laparotomy was performed, and the cecum was exteriorized to identify the terminal ileum. Briefly, the distal margin of the loop to transpose was selected as close as possible to the ileocecal valve, and the proximal margin was identified at ~10 cm from the distal margin. The bowel was then divided, leaving its mesenteric blood supply intact. The jejunum was interrupted just 10 cm distally from the ligament of Treitz, and the ileal loop was interposed and anastomosed isoperistaltically with the jejunal stumps (IT group $n = 10$). The sham operation (control group $n = 10$) comprised three enterotomies in the same locations as those in the IT group. The bowel was immediately reanastomosed after transection. Both operations lasted ~55 min per animal. When necessary, the sham operation was prolonged to produce a similar degree of operative stress. Postoperatively, rats received an analgesic for 2 days and had access to a liquid diet for 5 days. The rats then consumed a standard diet for 7 months. Body weight and food intake were recorded monthly after 2 months from the surgical procedure. At the end of 7 months, the rats were killed, and blood was collected for subsequent biochemical assays. Serum content of total cholesterol, HDL, triglycerides, and aspartate aminotransferase (AST) was measured by enzymatic assays (Wako Chemicals, Osaka, Japan). Hepatic and intestinal samples were snap frozen for RNA and protein isolation or fixed in formalin for histology. For histologic analysis, colon samples were fixed in buffered formalin, and routinely prepared 5-μm

sections were stained with hematoxylin and eosin and alcian blue as previously described (23).

**Animal protocols: treatments with chenodeoxycholic acid and oleanolic acid.** Seven months after the surgical procedure of ileal transposition, control and IT rats were randomized in two subgroups ($n = 5$) that received orally vehicle (methylcellulose 1%) or the FXR agonist chenodeoxycholic acid (CDCA) 20 mg/kg for 7 days. Rats were left unfed for 16 h and administered again with the FXR agonist. Three hours after the last administration of CDCA, blood glucose was measured in triplicate before and 20, 30, 40, 60, 80, 100, and 120 min after the administration of D-glucose solution (2 g/kg body weight) by oral gavage. Blood was obtained through the tail vein, and glucose was assessed with a glucometer. Blood samples were collected and insulin concentration was determined with a rat insulin ELISA kit (Mercodia). The animals were killed, and liver samples were excised and immediately snap frozen for RNA and protein isolation.

To investigate oleanolic acid effect on glucose and glucagon-like peptide 1 (GLP-1) release, both groups of rats were sedated with pentothal 50 mg/kg, and blood glucose was measured before and 15, 30, 45, and 60 min after the administration of oleanolic acid solution (10 g/kg body weight) by oral gavage. Insulin and GLP-1 levels were measured in plasma. Insulin and GLP-1 determination were performed as described below.

**Western blotting.** Frozen liver samples of ~100 mg obtained from the control rats (untreated or treated with CDCA) and from IT rats (untreated or treated with CDCA), were homogenized in 500 μL of T-PER (Pierce) supplemented with protease and phosphatase inhibitors. The homogenates were centrifuged at 10,000g for 10 min, and the supernatants were used as whole-cell lysates. Protein levels in tissue extract were quantified with Bradford reagent, and 20 μg of proteins were used in each SDS-PAGE run, which were subsequently transferred to nitrocellulose membranes (Bio-Rad) and probed with primary antibodies pERK 1/2-Thr202/Tyr204 (#9101S), ERK1/2 (#9102), pAKT-Ser473 (#9271), AKT (#9272), pGSK3β-Ser9 (#9336), and GSK3β (#9315P; all from Cell Signaling). Rabbit anti-IgG (Bio-Rad) was used as a secondary antibody, and specific protein bands were visualized by chemoluminescence with Supersignal West Dura reagent (Pierce). Quantification of the blots was performed with ImageJ software. For each sample, integrated density of the phospho-antibody band was divided by that of the total antibody band.

**Analysis of blood glucose, insulin, and GLP-1 levels and oral glucose tolerance test.** Oral glucose tolerance test (OGTT) was performed after 12–14 h of fasting (7 months after surgical procedure). To reduce the stress during blood collection, rats were sedated with pentothal (50 mg/kg). Blood glucose was measured in triplicate before (baseline) and 20, 30, 40, 60, 80, 100, and 120 min after the administration of D-glucose solution (2 g/kg body weight) by oral gavage. Blood was obtained by the tail vein, and glucose was assessed with a glucometer (OneTouch Ultra; LifeScan, Milpitas, CA). Blood samples were placed in centrifuge tubes containing 50 mmol/L EDTA and 100 μmol/L dipeptidyl peptidase 4 inhibitor that was added to avoid GLP-1 degradation. After centrifugation (3,000 rpm for 10 min at 4°C), plasma was collected and stored at −80°C until assay. Insulin concentration was determined with a rat insulin ELISA kit (Mercodia), and plasma levels of GLP-1 were measured with an enzyme immunosorbent assay kit (Phoenix Pharmaceuticals).

**Quantitative real-time PCR.** Immediately after kill, the liver and ileum were excised from the control and IT rats. Total RNA was isolated from these samples with TRIzol reagent (Invitrogen) according to manufacturer protocol. One microgram of purified RNA was treated with DNAse-I and reverse transcribed to cDNA with SuperScipt II (Invitrogen) in a 20-μL reaction volume with random primers. For quantitative real-time (RT) PCR, 25 ng of template was dissolved in a 25-μL solution containing 200 nmol/L of each primer and 12.5 μL of SYBR GreenER qPCR SuperMix (Invitrogen) for the iCycler iQ detection system (Bio-Rad). All reactions were performed in triplicate, and the thermal cycling conditions were as follows: 2 min at 50°C and 10 min at 95°C followed by 50 cycles of 95°C for 15 s, 58°C for 30 s, and 72°C for 30 s. The relative mRNA expression was calculated according to the cycle threshold method. All PCR primers were designed with Primer3 software (http://frodo.wi.mit.edu/primer3/) using published sequence data obtained from the National Center for Biotechnology Information database (Supplementary Table 1).

**Bile acids determination and sample preparation.** The stock solutions of the individual tauroconjugated and unconjugated bile acids were prepared separately in methanol at a concentration of 1 mg/mL. All stock solutions were stored at −20°C. Calibration standards were prepared by combining appropriate volumes of each bile acid stock solution and methanol. The calibration range was from 10 nmol/L to 100 μmol/L of each bile acid in the final solution. Rat serum sample aliquots of 100 μL were deproteinized with 1 mL cold acetonitrile (ACN) with 5% NH4OH, vortexing for 1 min (23). After centrifugation at 16,000g for 10 min, the clear supernatant was transferred to a new vial, snap frozen, and lyophilized. The sample was then redissolved in methanol and water (2:1 volume for volume [v/v]) for tauroconjugated bile acid

TABLE 1
Clinical and biochemical assessments 7 months after IT

| Parameter | Control group | IT group |
|---|---|---|
| Daily food intake (g/100 g body weight) | 4.62 ± 0.35 | 5.32 ± 0.41 |
| Final weight (g) | 616.1 ± 31.6 | 580 ± 42.1 |
| Glucose (mg/dL) | 79.2 ± 1.3 | 72.64 ± 2.35 |
| Cholesterol (mg/dL) | 78.33 ± 4.0 | 85.33 ± 4.8 |
| HDL cholesterol (mg/dL) | 65.17 ± 3.8 | 64.83 ± 8.5 |
| Triglycerides (mg/dL) | 62.5 ± 5.7 | 38.8 ± 8.0* |
| AST (units/L) | 82.5 ± 3.7 | 85.3 ± 4.7 |

Data are mean ± SE. $n = 10$. *$P < 0.05$ IT vs. sham.

determination and in methanol-ammonium acetate 10 mmol/L with 0.005% formic acid (3:2 v/v) for unconjugated bile acid determination. A bile acid extraction yield of 95% was measured with the addition of bile acid standard in plasma samples before and after the deproteinization procedure. For colon and liver samples, 100 mg of lyophilized tissue was homogenized for 20 min in 10 mL $H_2O$. After 45 min of sedimentation, 500 μL of liver homogenate was added to 2 mL of ice-cold alkaline ACN. Samples were vortexed and shaken continuously for 30 min and then centrifuged at 16,000$g$ for 10 min. The supernatant was aspirated, and the pellet was extracted with another 1 mL of ice-cold alkaline ACN. Supernatants from the two extraction steps were pooled, lyophilized, and reconstituted in 100 μL of methanol and water (2:1 v/v) for tauroconjugated bile acid determination and in 100 μL of methanol-ammonium acetate 10 mmol/L with 0.005% formic acid (3:2 v/v) for unconjugated bile acid determination (24).

**Liquid chromatography and mass spectrometry.** For liquid chromatography-tandem mass spectrometry (MS/MS) analysis, chromatographic separation was carried out on the LTQ XL high-performance liquid chromatography mass spectrometry system (ThermoScientific) equipped with the Accelera 600 Pump and Accelera AutoSampler system. The mixture was separated on a Jupiter 5 μm C18 Å column (150 × 2.00 mm) (Phenomenex). Tauroconjugated bile acids were separated at a flow rate of 200 μL/min with a methanol-aqueous ammonium acetate gradient (25). Mobile phase A was 5% methanol in water containing 2 mmol/L ammonium acetate at pH 7; mobile phase B was methanol containing ammonium acetate at 2 mmol/L. The gradient started at 30% B and increased to 100% B in 20 min, kept at 100% B for 5 min, and then decreased to 30% B in 1 min and kept at 30% B for 10 min. Electrospray ionization was performed in negative ion mode; the ion source temperature was set at 280°C. The tune page parameters were automatically optimized by injecting taurocholic acid (TCA) at 1 μmol/L as the standard. The MS/MS detection was operated in multiple reaction monitoring (MRM) mode using a collision energy of 20 (arbitrary units), and the observed transitions were as follows: tauro-β-muricholic acid (TβMCA) at 13.5 min MRM of 514.28 Th→514.28 Th, taurohyocholic acid (THCA) at 15.6 min MRM of 498.29 Th→498.29 Th, TCA at 16.6 min MRM of 514.28 Th→514.28 Th, taurochenodeoxycholic acid (TCDCA) at 18.5 min MRM of 498.29 Th→498.29 Th, and taurodeoxycholic acid (TDCA) at 18.9 min MRM of 498.29 Th→498.29 Th.

Unconjugated bile acids were separated at a flow rate of 200 μL/min. Mobile phase A was 10 mmol/L ammonium acetate in water containing 0.005% formic acid; mobile phase B was 10 mmol/L ammonium acetate in methanol containing 0.005% formic acid (26). The gradient program started at 60% B and increased to 95% B in 25 min, kept at 95% B for 9 min, and then decreased to 60% B in 1 min and kept at 60% B for 10 min. Electrospray ionization was performed in negative ion mode; the ion source temperature was set at 280°C (27). The tune page parameters were automatically optimized by injecting cholic acid (CA) at 1 μmol/L as the standard. The MS/MS detection was operated in MRM mode using a collision energy of 15 (arbitrary units), and the observed transitions were as follows: HCA at 8.9 min MRM of 391.29 Th→391.29 Th, CA at 10.2 min MRM of 407.28 Th→407.28 Th, CDCA at 13.8 min MRM of 391.29 Th→391.29 Th, deoxycholic acid (DCA) at 14.4 min MRM of 391.29 Th→391.29 Th, and lithocholic acid (LCA) at 17.5 min MRM of 375.28 Th→375.28 Th.

**Tissue triglyceride and cholesterol determination.** For hepatic and ileal determination of triglyceride and cholesterol levels, fragments of ~100 mg of liver and ileum were homogenized with 1 mL of T-PER. The homogenates were used for protein concentration analysis (Bradford assay; Bio-Rad) and 100 μL of tissue extracts added to 1.6 mL chloroform:methanol (2:1) for 16 h at 4°C, after which 200 μL of 0.6% NaCl was added and the solution centrifuged at 2,000$g$ for 20 min. The organic layer was removed and air dried in a chemical hood. The resulting pellet was dissolved in 400 μL PBS containing 1% Triton X-100 (Sigma-Aldrich). Triglyceride and cholesterol levels were measured by specific enzymatic reagents (Wako Chemicals, Osaka, Japan).
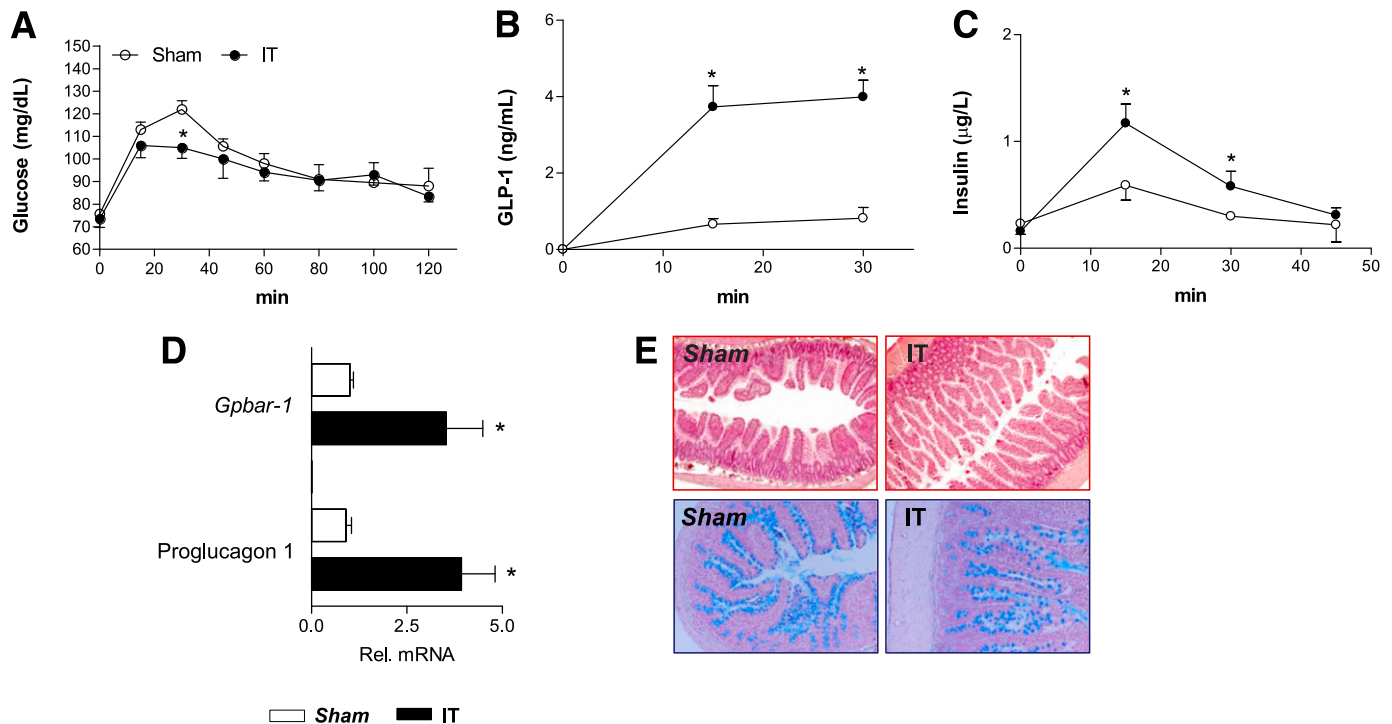


FIG. 1. IT rats show an improvement in glucose tolerance. OGTT performed at 7 months after the surgical procedure in IT and sham-operated rats after 18 h of food withdrawal (fasting). *A*: Blood glucose curve. *B*: Plasma levels of GLP-1. *C*: Plasma levels of insulin. *D*: Ileal gene expression of *Gpbar-1* and proglucagon 1. Values are normalized relative to *Gapdh* mRNA and are expressed relative to those of sham-operated rats, which were arbitrarily set to 1. Data are mean ± SE ($n = 5$ per group). *E*: Representative hematoxylin-eosin and alcian blue staining of ileal section obtained from sham-operated and IT rats. *$P < 0.05$ IT vs. sham.

**Statistical analysis.** All values are expressed as mean ± SE of the number of observations per group. Comparisons of more than two groups were made with one-way ANOVA with post hoc Tukey test. Comparison of two groups was made with Student $t$ test for unpaired data, when appropriate. Differences were considered to be statistically significant at $P < 0.05$.

## RESULTS

**Effects of IT surgery on systemic and biochemical parameters.** Over the 7 months postsurgery, all rats (sham and IT) consumed a similar amount of diet, and there was no significant difference in body weight between the two groups (Table 1). Although similar plasma levels of total cholesterol, HDL, AST, and glucose were observed, a strong reduction of plasma levels of triglycerides was documented in IT rats, consistent with previous works (28–30) (Table 1). Glucose tolerance was significantly improved at 15 and 30 min in IT rats (Fig. 1A). Moreover, GLP-1 and insulin levels were significantly higher in IT rats than in sham-operated rats (Fig. 1B and C). Because IT surgery is recognized to increase the secretion of GLP-1, a well-defined target gene for the bile acid–activated plasma membrane receptor GPBAR1, we examined the mRNA levels of *Gpbar-1* and proglucagon 1 (a GLP-1 precursor) in the ileum. Results from these experiments demonstrated that both *Gpbar-1* and proglucagon 1 genes

were induced in the ileum of IT rats (Fig. 1D). The histopathological analysis of ileum sections demonstrated an increase in length and number of villi in the interposed ileal segment compared with the ileum of the sham-operated rats (Fig. 1E). The role of GPBAR1 was further investigated by challenging sham-operated and IT rats with oleanolic acid, a GPBAR1 ligand. These functional studies demonstrated that treating rats with oleanolic acid–activated intestinal *Gpbar-1* induced a rapid and robust increase of GLP-1 and insulin, thus improving the glucose profile in response to OGTT (Supplementary Fig. 1).

**Serum bile acids.** We next investigated the bile acid composition in the plasma, liver, and small intestine in IT rats. Consistent with previous works (28,31,32), we found that IT increases the total plasma levels of bile acids (Fig. 2A). The plasma concentrations of nonconjugated bile acids, CDCA, CA, and HCA were significantly increased in IT rats (Fig. 2B). Moreover, IT surgery significantly increased plasma concentration of tauro-β-muricholic acid (TβMCA) and TCDCA but reduced that of TDCA (Fig. 2C). When these changes were expressed as a percentage of total bile acids, IT rats had a robust increase in the percentage of primary bile acids CDCA, CA, and HCA (4, 17, and 42%, respectively) compared with sham-operated rats (1, 6, and 24%). Moreover, as shown in Fig. 2D and E,
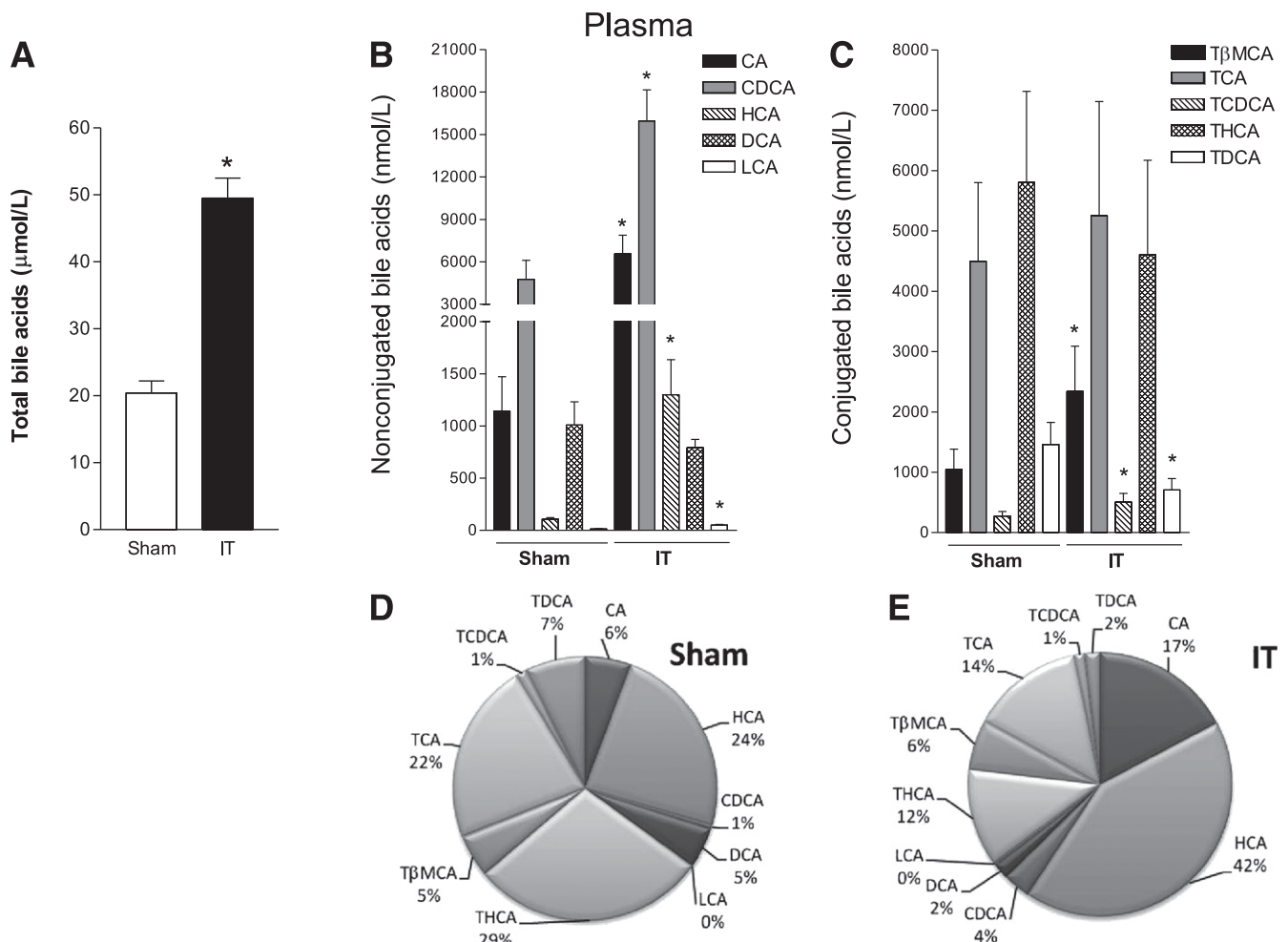


FIG. 2. Characterization of plasma bile acid concentrations. *A*: Total bile acids. *B*: Nonconjugated bile acids CA, CDCA, HCA, DCA, and LCA. *C*: Conjugated bile acids TβMCA, TCA, TCDCA, THCA, and TDCA. *D* and *E*: Qualitative analysis of bile acid composition in sham-operated and IT rats, respectively. Data are mean ± SE (*n* = 5 per group). *$P < 0.05$ IT vs. sham.

a reduction in the percentage of tauroconjugated bile acids TCA, TDCA, and THCA was found in the IT group (14, 2, and 12%, respectively) compared with the sham-operated group (22, 7, and 29%).

**Hepatic bile acids.** In the contrast to that observed in the serum, hepatic levels of total bile acids were lower in IT rats than in sham-operated rats (Fig. 3A). The analysis of quantitative distribution of bile acids in the liver highlighted that the concentration of primary bile acids CA and HCA increased in IT rats (Fig. 3B). Furthermore, the concentration of tauroconjugated bile acids TCDCA and TDCA were enhanced, whereas that of TCA was strongly reduced after bariatric surgery (Fig. 3C). Of note, the compositional analysis of plasma bile acids expressed as a percentage showed that ~95% of bile acids in the liver were tauroconjugated in both experimental groups and confirmed that IT surgery enhanced the hepatic content of THCA (23 vs. 4%, IT vs. sham, respectively) and reduced hepatic levels of TCA (49 vs. 84%).

**Ileal bile acids.** IT reduces the total bile acid content in the intestinal wall, a measure of bile acid absorption by the intestine (Fig. 4A). Thus, although the intestinal content of CDCA, CA, and LCA was higher in the IT group than in the

sham-operated group (Fig. 4B), the intestinal concentration of conjugated bile acids TCA, TDCA, and THCA was significantly reduced in IT rats compared with sham-operated rats (Fig. 4C). As in the liver, the analysis of intestinal bile acids showed that ~95% were tauroconjugated in both groups. In particular, the percentage of TCA and THCA (FXR and LXRα agonists, respectively) did not change between the two groups, whereas that of TβMCA (a TGR5 ligand) and CA increased after IT (Fig. 4D and E).

**IT dissociates intestinal and liver FXR activities.** Having found that surgical interposition of the distal ileum into the proximal jejunum strongly decreases hepatic content of TCA (a well-recognized FXR agonist in rodents) but does not change its intestinal content, we investigated whether this shift in relative bile acid composition modulates the expression of FXR and its target genes in both the ileum and the liver of IT rats. RT-PCR data analysis demonstrated that the IT procedure upregulates the expression of *Fxr* and its target genes *Ostα* and *Fgf15* in the ileum (Fig. 5A). Because *Fgf15* inhibits hepatic gluconeogenesis through a pathway involving the inhibition of PGC-1α, a coactivator of the nuclear receptor glucocorticoid receptor (GR), the master regulator of gluconeogenic genes
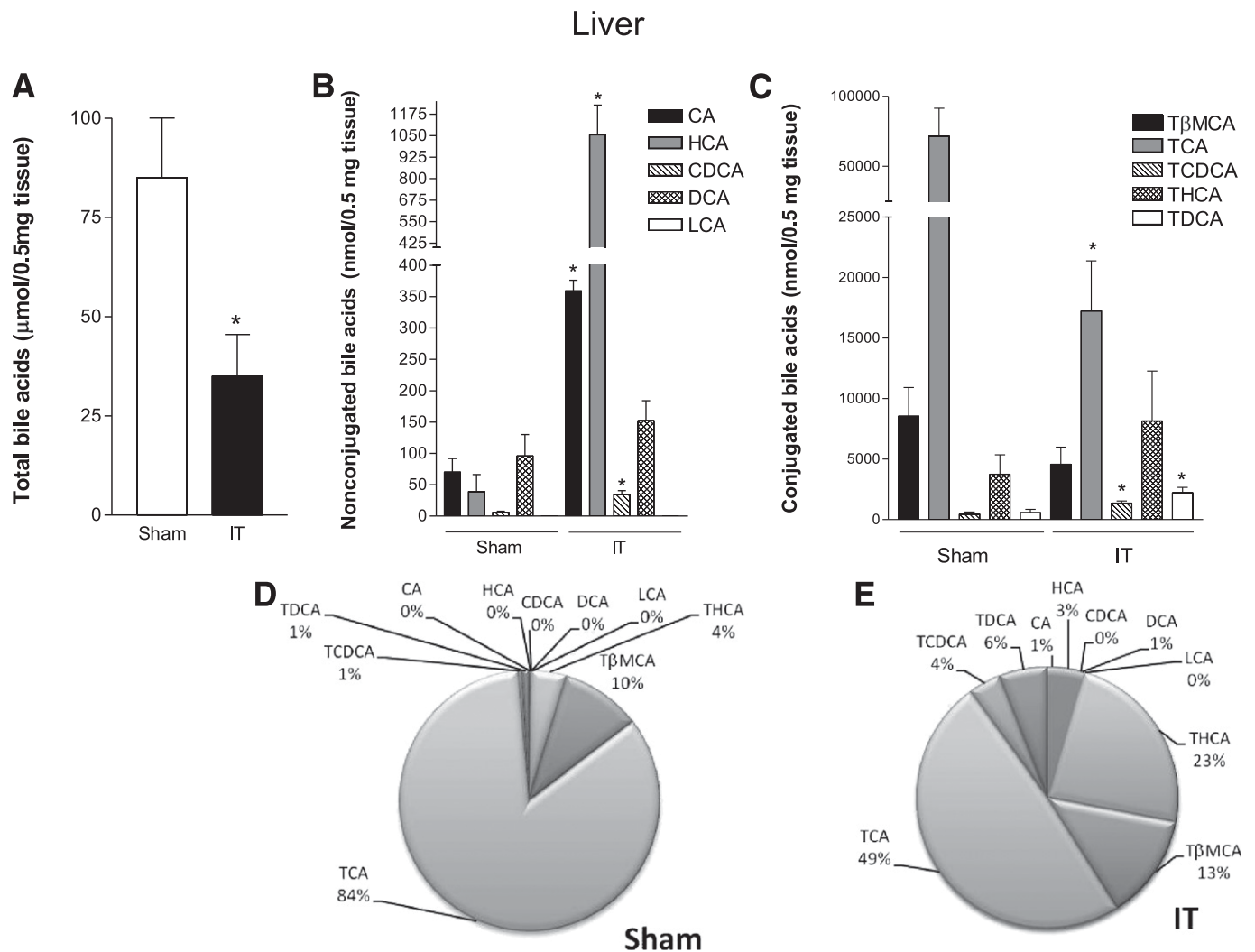
## Liver



FIG. 3. Characterization of hepatic bile acid concentrations. *A*: Total bile acids. *B*: Nonconjugated bile acids CA, HCA, CDCA, DCA, and LCA. *C*: Conjugated bile acids TβMCA, TCA, TCDCA, THCA, and TDCA. *D* and *E*: Qualitative analysis of bile acid composition in sham-operated and IT rats, respectively. Data are mean ± SE (*n* = 5 per group). *P < 0.05 IT vs. sham.
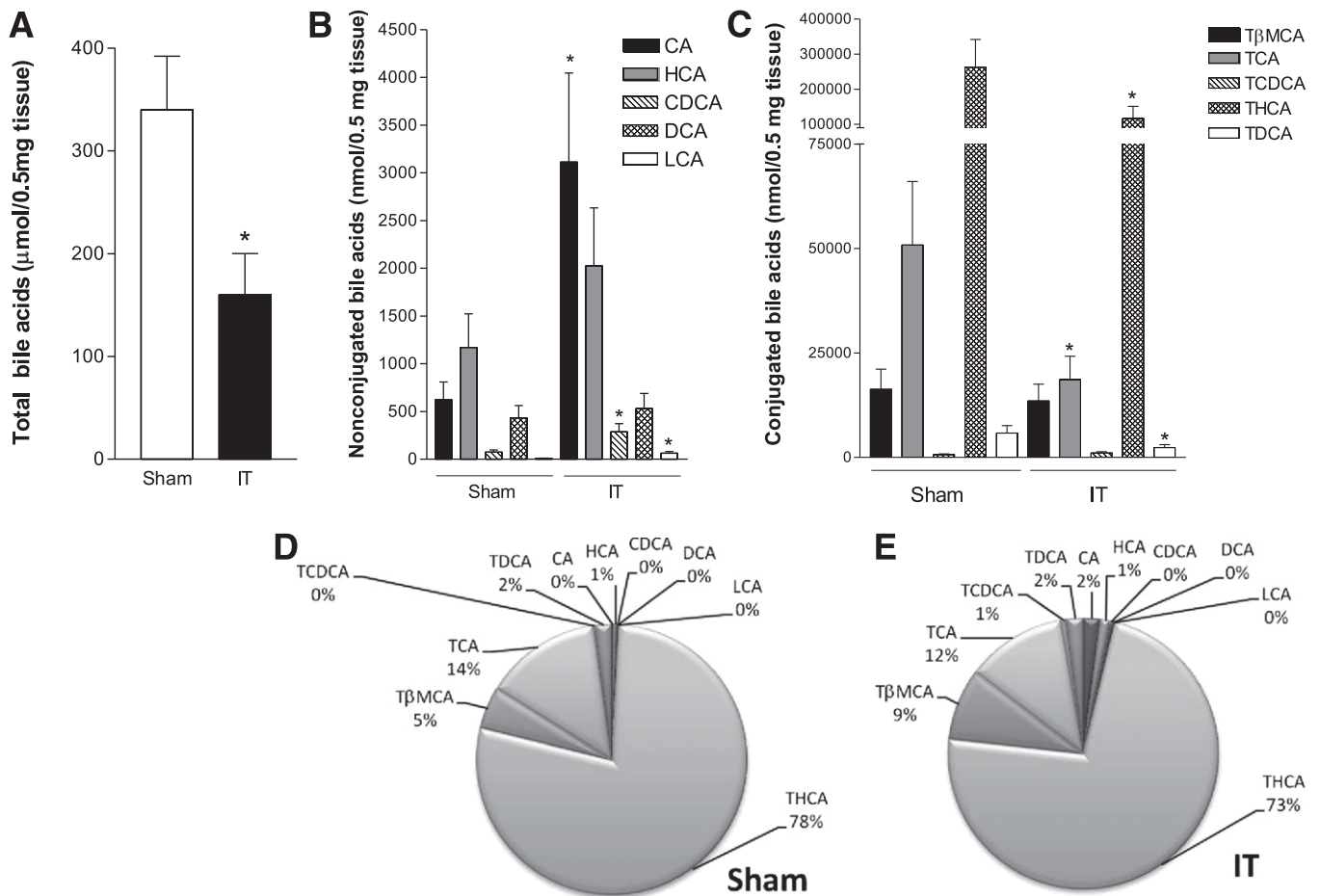
## Ileum



FIG. 4. Characterization of ileal bile acid concentrations. *A*: Total bile acids. *B*: Nonconjugated bile acids CA, HCA, CDCA, DCA, and LCA. *C*: Conjugated bile acids TβMCA, TCA, TCDCA, THCA, and TDCA. *D* and *E*: Qualitative analysis of bile acid composition in sham-operated and IT rats, respectively. Data are mean ± SE (*n* = 5 per group). *$P < 0.05$ IT vs. sham.

*G6PC* and *PEPCK* (9,33,34), we investigated the FXR/FGF15 pathway in sham-operated and IT rats. For this purpose, we performed an OGTT in IT rats treated for 7 days with the natural FXR agonist CDCA. On the 7th day, rats were fasted overnight and treated with CDCA 3 h before the OGTT. Results demonstrated that administering IT rats with CDCA improves the glucose tolerance at all time points, with the greatest differences observed between 60 and 120 min (Supplementary Fig. 2*A*). Furthermore, compared with sham-operated rats, administering IT rats with CDCA resulted in a robust reduction of plasma levels of insulin (Supplementary Fig. 2*B*). The IT surgery per se increased intestinal expression of *Fgf15* (Fig. 5*A*), and exposure to CDCA resulted in a further approximately sixfold induction of this hormone (Supplementary Fig. 2*C*). These changes resulted in a robust suppression of gluconeogenetic genes in the liver. Thus, IT surgery resulted in a robust reduction of *Pepck*, *G6pc*, and *Pgc-1α* mRNA expression in the liver (Fig. 5*B*), and exposure to CDCA further amplified this effect (Supplementary Fig. 2*D*), whereas no changes in hepatic expression of *Gr* was observed (Fig. 5*B* and Supplementary Fig. 2*D*). Because these findings suggest that the activation of the intestinal FXR/FGF15 axis regulates hepatic gluconeogenesis in IT rats, we further dissected the FGF15 and insulin signals in

the liver by investigating the phosphorylation status of ERK, AKT, and GSK3β by Western blot analysis (Supplementary Fig. 3*A*). Results demonstrated that CDCA significantly reduces GSK3β phosphorylation while enhancing the phosphorylation of ERK1/2 on both Thr 202 and Tyr 204 residues (Supplementary Fig. 3*B*). Moreover, AKT phosphorylation was not changed (Supplementary Fig. 3*B*) (34).

The investigation of *Fxr* gene expression in the liver also revealed that IT surgery has no effect on the transcription of this nuclear receptor as well as that of its canonical target genes *Shp* and *Bsep*, whereas expression of *Ostα*, another FXR target gene, was repressed by ~70% (Fig. 5*C*). Similarly to *Ostα*, RT-PCR results showed that the liver expression of genes involved in bile acid uptake (i.e., *Ntcp*) and synthesis (*Cyp7α1*, *Cyp8β1*, *Cyp27Aα1*, and *Cyp7β1*) is reduced by 60–80% by IT surgery.

**IT dissociates intestinal and liver LXR activities.** Because the IT surgery increased the concentration of THCA, a ligand for LXRα, we analyzed both ileal and hepatic expression of LXRα, the main regulator of RCT and lipogenesis. As illustrated in Fig. 6*A*, the IT surgery resulted in a robust induction of *Lxrα* and its target genes *Abca1*, *Abcg5*, and *Abcg8*, which are involved in the RCT pathway (15,16). It has been reported that intestinal-specific LXRα
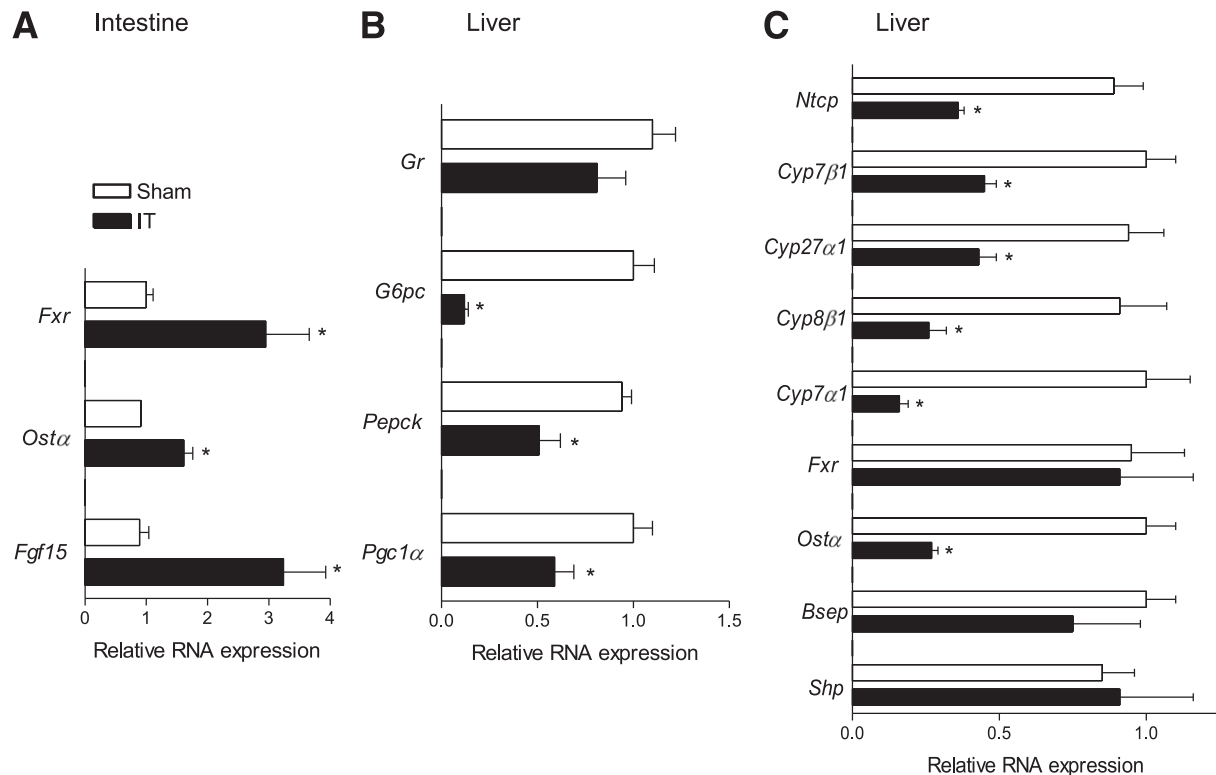
**FIG. 5. IT dissociates ileal and hepatic FXR expression/activity. A: Ileal mRNA relative expression of Fxr, Ostα, and Fgf15. B: Hepatic mRNA relative expression of Pepck, G6pc, Pgc1α, and Gr. C: Hepatic mRNA expression of Fxr, Shp, Ntcp, Cyp7α1, Cyp7β1, Cyp8β1, Cyp27α1, Bsep, and Ostα. Values are normalized relative to Gapdh mRNA and are expressed relative to those of sham-operated rats, which were arbitrarily set to 1. Data are mean ± SE (n = 5 per group). *P < 0.05 IT vs. sham.**

activation leads to decreased intestinal cholesterol absorption and an improved lipoprotein profile (35), but we did not observed any reduction of plasma cholesterol levels in IT rats (Table 1). However, IT rats had a significant reduction in the expression of the *Lxrα* target gene *Npc1l1*, a central player in intestinal cholesterol absorption (36,37). Of note, the investigation of fatty acid transport protein 4 (*Fatp4*), which is the principal fatty acid transporter in enterocytes (37,38) as well as that of *Cd36*, another LXRα-regulated gene involved in the uptake of oxidized LDL, revealed that the expression of these proteins is not changed between sham-operated and IT rats (Fig. 6A).

As shown in Fig. 6B, the analysis of hepatic expression of *Lxrα* demonstrated that this transcription factor and its target gene *Cd36* are reduced in the liver of IT rats, although no change was observed in the hepatic expression of other LXRα target genes, such as *Abca1*, *Abcg5*, and *Abcg8*. In line with these results, the hepatic mRNA expression of the LXRα target gene *Srebp1c*, the main regulator of *Fas* expression, was reduced after the surgical procedure (Fig. 6B).

We found no significant changes in terms of hepatic and ileal content of cholesterol and triglycerides between the experimental groups (Fig. 6C–E). Of note, ileal triglyceride content was strongly upregulated in IT rats compared with sham-operated rats (Fig. 6F).

## DISCUSSION

Bariatric surgery, such as Roux-en-Y gastric bypass, is currently the most effective long-term treatment for obesity (39,40) and has been shown to markedly improve glucose homeostasis in type 2 diabetes (41–43), but the mechanisms by which this occurs remain poorly defined. The improvement of glucose homeostasis after bariatric surgery has been attributed to weight loss resulting from a reduction in gastric volume and/or reduced nutrient absorption, depending on the type of surgery. However, results from clinical studies support a role for adaptive endocrine changes. First, in patients with type 2 diabetes undergoing bariatric surgery, such as Roux-en-Y gastric bypass, glucose normalization often occurs before substantial weight loss (43,44). Second, bariatric surgeries involving bypass of the proximal small intestine, such as IT and biliopancreatic diversion, are more effective at decreasing obesity and reversing type 2 diabetes than bariatric surgeries involving only gastric restriction (43,45). These observations have led to the concept that the release of insulinotropic hormones, such as GLP-1 and PYY, from L cells located in the distal ileum plays an important mechanistic role (46). Increased secretion of these hormones after bariatric surgery has been demonstrated in a number of clinical studies and may contribute to weight loss and improved glucose metabolism (45–47).

In the current study, we investigated the molecular mechanisms that underlie the metabolic benefits induced by ileal transposition, a surgical procedure in which the distal ileum is interposed in the proximal jejunum in an isoperistaltic direction. The results demonstrate that IT improves glucose homeostasis and lipid metabolism by altering the physiology of bile acids. In particular, IT increases the total concentration of plasma bile acids while reducing their content in the intestinal wall and liver.
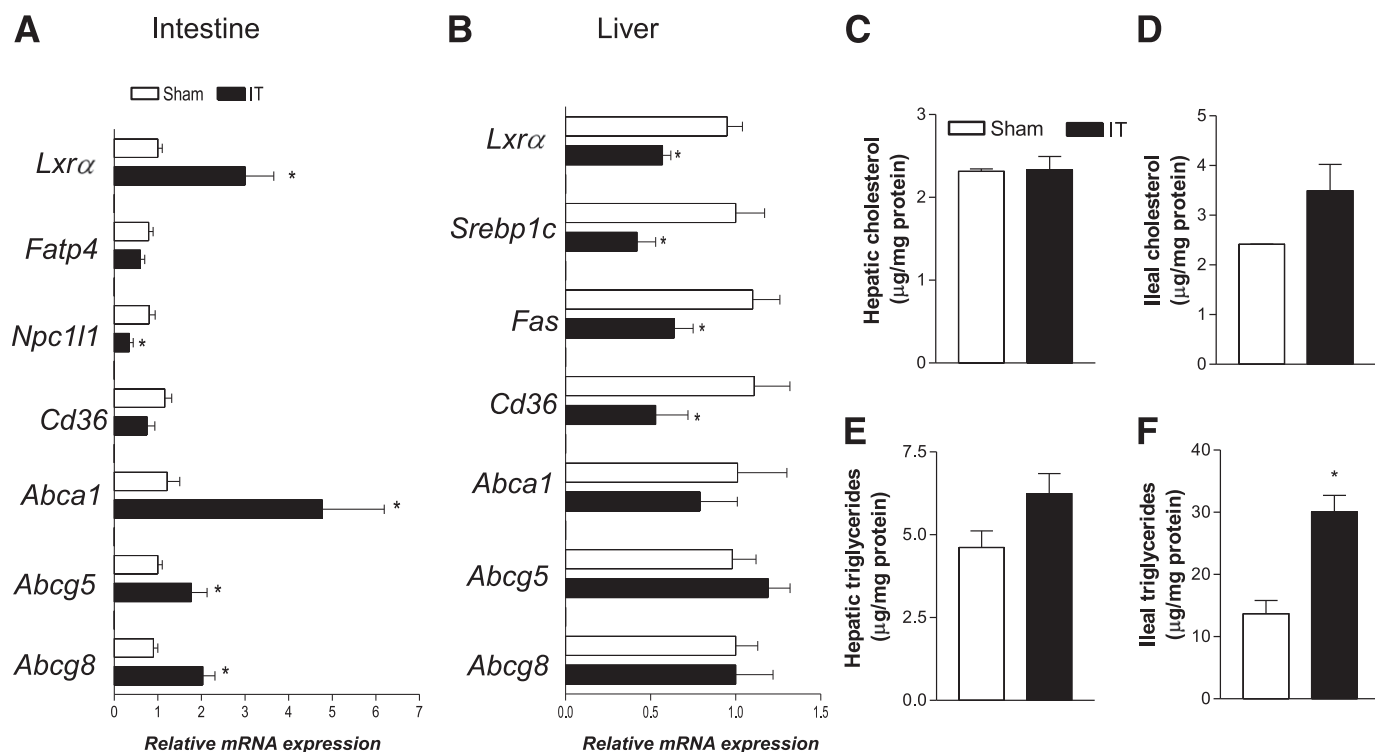
FIG. 6. IT dissociates ileal and hepatic LXR expression/activity. *A*: RT-PCR analysis of ileal expression of *Lxrα*, *Fatp4*, *Npc1l1*, *Cd36*, *Abca1*, *Abcg5*, and *Abcg8*. *B*: RT-PCR analysis of hepatic expression of *Lxrα*, *Srebp1c*, *Fas*, *Cd36*, *Abca1*, *Abcg5*, and *Abcg8*. Values are normalized relative to *Gapdh* mRNA and are expressed relative to those of sham-operated rats, which are arbitrarily set to 1. Cholesterol and triglyceride concentrations in the liver (*C* and *E*) and intestine (*D* and *F*) of sham-operated and IT rats. Data are mean ± SE (*n* = 5 per group). *$P < 0.05$ IT vs. sham.

Compositional analysis of the hepatic bile acid pool revealed that the IT surgery reduces the percentage of TCA, a well-recognized FXR agonist; enhances that of THCA, a well-identified LXRα agonist; and has no effect on βMCA, a recognized TGR5 agonist. In contrast, the relative amount of FXR and LXRα agonists in the intestine remains constant, but the amount of βMCA is increased in the ileum of IT rats. These findings raise the concept that by resetting the composition of bile acids in enterohepatic tissues or by increasing the cycling of bile acids from the intestine to the liver (i.e., enterohepatic cycling), IT can reset the expression and activity of bile acid–activated receptors (i.e., *Gpbar-1*, *Fxr*, and *Lxrα*) throughout the whole intestine. To confirm this hypothesis we examined whether IT regulates intestinal GPBAR-1 expression/activity and demonstrated that its mRNA expression increased after the surgical procedure and that the relative increase of βMCA, a GPBAR-1 agonist, was likely responsible for GPBAR-1–mediated secretion of GLP-1 in the intestine of IT rats.

A key observation of the current study is that IT exerts opposite effects on FXR signaling in the intestine and liver. The results demonstrate that although ileal expression of *Fxr* and its target genes *Ostα* and *Fgf15* increases in response to IT, the expression *Fxr* and its target genes (*Ostα*, *Bsep*, and *Shp*) in the liver is downregulated or remains unchanged. Together with the fact that hepatic bile acid concentrations are dramatically reduced by IT, these data indicate that this surgical procedure activates the expression/activity of ileal FXR while its activity in the liver is repressed. This finding was further confirmed by the analysis of genes involved in liver metabolism of bile acids. Thus, the liver expression of genes involved in bile

acid uptake (i.e., *Ntcp*) and bile acid synthesis (e.g., *Cyp7α1*, *Cyp8β1*, *Cyp27Aα1*, *Cyp7β1*) are reduced by 60–80% by IT. Because these genes are directly regulated by intracellular concentrations of bile acids, the fact that bile acid synthesis is repressed, despite the robust reduction of liver bile acid concentrations caused by IT, indicates that IT induces an escape mechanism that superimposes liver FXR. Indeed, regulation of *Cyp7α1* and *Cyp8β1* by FXR is mediated by the activation of several indirect mechanisms (34,48,49). FXR-mediated activation of SHP and *Fgf15* (FGF19 in humans) has been shown to be responsible for this suppression. By using novel genetically modified mice, Kong et al. (49) showed that the intestinal FXR/FGF15 pathway is critical for suppressing both *Cyp7α1* and *Cyp8β1* gene expression, whereas the liver FXR/SHP pathway plays a minor role in suppressing *Cyp7α1* gene expression. Present data are fully consistent with these findings and indicate that IT causes a selective activation of intestinal FXR and that the FXR/FGF15 pathway mediates, in turn, the repression of bile acid synthesis observed in this study.

Another important observation from this study is that the activation of the intestinal FXR/FGF15 axis represses hepatic gluconeogenesis. Indeed, the FXR-mediated induction of *Fgf15* in the intestine resulted in a strong downregulation of the expression of two gluconeogenic genes, *G6pc* and *Pepck*, in the liver of IT rats. In addition, administering rats with CDCA increased ERK1/2 phosphorylation while reducing GSK3β phosphorylation. Because previous work reported that FGF19 (a human ortholog of FGF15) induces glycogen synthesis by enhancing ERK1/2 phosphorylation and repressing that of GSK3β (50), the present results suggest that the FXR-mediated induction

of FGF15 could also induce glycogen synthesis. Thus, the selective inhibition of hepatic activity of FXR achieved by the surgical strategy may be an appealing option for the therapy of obesity and the diseases related to dysfunctions of glucose homeostasis.

IT surgery also dissociates the expression/activity of LXRs. In this regard, we observed that IT modulates *Lxrα* expression and activity. Moreover, we found that the increased expression of *Lxrα* in the ileum was associated with an upregulation of LXRα target genes *Abca1*, *Abcg5*, and *Abcg8* and with a repression of *Npc1l1*, a protein that mediates the cholesterol absorption in the intestine. Of note, the expression of *Fatp4*, the main mediator of intestinal absorption of triglycerides, as well as that of *Cd36*, which mediates the absorption of oxidized LDL, was not changed between sham-operated and IT rats. According to RT-PCR data, IT rats had a robust increase in the intestinal content of triglycerides.

In conclusion, this study demonstrated that IT, a bariatric surgery, produces improvements of glucose tolerance and obesity by altering the homeostasis of bile acids in rats. The altered physiology of bile acids results in extensive remodeling of expression/activity of bile acid–activated receptors in enterohepatic tissues. These data unveil potential novel strategies for the prevention and treatment of obesity and type 2 diabetes.

## REFERENCES

1. Calkin AC, Tontonoz P. Transcriptional integration of metabolism by the nuclear sterol-activated receptors LXR and FXR. Nat Rev Mol Cell Biol 2012;13:213–224
2. Kalaany NY, Mangelsdorf DJ. LXRS and FXR: the yin and yang of cholesterol and fat metabolism. Annu Rev Physiol 2006;68:159–191
3. Goodwin B, Jones SA, Price RR, et al. A regulatory cascade of the nuclear receptors FXR, SHP-1, and LRH-1 represses bile acid biosynthesis. Mol Cell 2000;6:517–526
4. Lu TT, Makishima M, Repa JJ, et al. Molecular basis for feedback regulation of bile acid synthesis by nuclear receptors. Mol Cell 2000;6:507–515
5. Chen F, Ma L, Dawson PA, et al. Liver receptor homologue-1 mediates species- and cell line-specific bile acid-dependent negative feedback regulation of the apical sodium-dependent bile acid transporter. J Biol Chem 2003;278:19909–19916
6. Grober J, Zaghini I, Fujii H, et al. Identification of a bile acid-responsive element in the human ileal bile acid-binding protein gene. Involvement of the farnesoid X receptor/9-cis-retinoic acid receptor heterodimer. J Biol Chem 1999;274:29749–29754
7. Landrier JF, Eloranta JJ, Vavricka SR, Kullak-Ublick GA. The nuclear receptor for bile acids, FXR, transactivates human organic solute transporter-α and -β genes. Am J Physiol Gastrointest Liver Physiol 2006;290: G476–G485
8. Fiorucci S, Cipriani S, Baldelli F, Mencarelli A. Bile acid-activated receptors in the treatment of dyslipidemia and related disorders. Prog Lipid Res 2010;49:171–185
9. Renga B, Mencarelli A, D'Amore C, et al. Glucocorticoid receptor mediates the gluconeogenic activity of the farnesoid X receptor in the fasting condition. FASEB J 2012;26:3021–3031
10. Lefebvre P, Cariou B, Lien F, Kuipers F, Staels B. Role of bile acids and bile acid receptors in metabolic regulation. Physiol Rev 2009;89:147–191
11. Prawitt J, Abdelkarim M, Stroeve JH, et al. Farnesoid X receptor deficiency improves glucose homeostasis in mouse models of obesity. Diabetes 2011; 60:1861–1871
12. Watanabe M, Houten SM, Wang L, et al. Bile acids lower triglyceride levels via a pathway involving FXR, SHP, and SREBP-1c. J Clin Invest 2004;113: 1408–1418
13. Schaap FG. Role of fibroblast growth factor 19 in the control of glucose homeostasis. Curr Opin Clin Nutr Metab Care 2012;15:386–391
14. Inagaki T, Choi M, Moschetta A, et al. Fibroblast growth factor 15 functions as an enterohepatic signal to regulate bile acid homeostasis. Cell Metab 2005;2:217–225
15. Repa JJ, Turley SD, Lobaccaro JA, et al. Regulation of absorption and ABC1-mediated efflux of cholesterol by RXR heterodimers. Science 2000; 289:1524–1529
16. Repa JJ, Berge KE, Pomajzl C, Richardson JA, Hobbs H, Mangelsdorf DJ. Regulation of ATP-binding cassette sterol transporters ABCG5 and ABCG8 by the liver X receptors α and β. J Biol Chem 2002;277:18793–18800
17. Chiang JY, Kimmel R, Stroup D. Regulation of cholesterol 7alpha-hydroxylase gene (CYP7A1) transcription by the liver orphan receptor (LXRalpha). Gene 2001;262:257–265
18. Peet DJ, Turley SD, Ma W, et al. Cholesterol and bile acid metabolism are impaired in mice lacking the nuclear oxysterol receptor LXR α. Cell 1998; 93:693–704
19. Repa JJ, Liang G, Ou J, et al. Regulation of mouse sterol regulatory element-binding protein-1c gene (SREBP-1c) by oxysterol receptors, LXRalpha and LXRbeta. Genes Dev 2000;14:2819–2830
20. Schultz JR, Tu H, Luk A, et al. Role of LXRs in control of lipogenesis. Genes Dev 2000;14:2831–2838
21. Zhou J, Febbraio M, Wada T, et al. Hepatic fatty acid transporter Cd36 is a common target of LXR, PXR, and PPARgamma in promoting steatosis. Gastroenterology 2008;134:556–567
22. Fazel I, Pourshams A, Merat S, Hemayati R, Sotoudeh M, Malekzadeh R. Modified jejunoileal bypass surgery with biliary diversion for morbid obesity and changes in liver histology during follow-up. J Gastrointest Surg 2007;11:1033–1038
23. Cipriani S, Mencarelli A, Chini MG, et al. The bile acid receptor GPBAR-1 (TGR5) modulates integrity of intestinal barrier and immune response to experimental colitis. PLoS ONE 2011;6:e25637
24. Huang J, Bathena SP, Csanaky IL, Alnouti Y. Simultaneous characterization of bile acids and their sulfate metabolites in mouse liver, plasma, bile, and urine using LC-MS/MS. J Pharm Biomed Anal 2011;55: 1111–1119
25. Bobeldijk I, Hekman M, de Vries-van der Weij J, et al. Quantitative profiling of bile acids in biofluids and tissues based on accurate mass high resolution LC-FT-MS: compound class targeting in a metabolomics workflow. J Chromatogr B Analyt Technol Biomed Life Sci 2008;871:306–313
26. Xiang X, Han Y, Neuvonen M, Laitila J, Neuvonen PJ, Niemi M. High performance liquid chromatography-tandem mass spectrometry for the determination of bile acid concentrations in human plasma. J Chromatogr B Analyt Technol Biomed Life Sci 2010;878:51–60
27. Alnouti Y, Csanaky IL, Klaassen CD. Quantitative-profiling of bile acids and their conjugates in mouse liver, bile, plasma, and urine using LC-MS/MS. J Chromatogr B Analyt Technol Biomed Life Sci 2008;873:209–217
28. Kohli R, Kirby M, Setchell KD, et al. Intestinal adaptation after ileal interposition surgery increases bile acid recycling and protects against obesity-related comorbidities. Am J Physiol Gastrointest Liver Physiol 2010;299:G652–G660
29. De Paula AL, Stival AR, Halpern A, et al. Improvement in insulin sensitivity and β-cell function following ileal interposition with sleeve gastrectomy in type 2 diabetic patients: potential mechanisms. J Gastrointest Surg 2011; 15:1344–1353
30. Cummings BP, Strader AD, Stanhope KL, et al. Ileal interposition surgery improves glucose and lipid metabolism and delays diabetes onset in the UCD-T2DM rat. Gastroenterology 2010;138:2437–2446, 2446.e1
31. Culnan DM, Albaugh V, Sun M, Lynch CJ, Lang CH, Cooney RN. Ileal interposition improves glucose tolerance and insulin sensitivity in the obese Zucker rat. Am J Physiol Gastrointest Liver Physiol 2010;299:G751– G760
32. Patti ME, Houten SM, Bianco AC, et al. Serum bile acids are higher in humans with prior gastric bypass: potential contribution to improved glucose and lipid metabolism. Obesity (Silver Spring) 2009;17:1671– 1677

33. Fu L, John LM, Adams SH, et al. Fibroblast growth factor 19 increases metabolic rate and reverses dietary and leptin-deficient diabetes. Endocrinology 2004;145:2594–2603

34. Potthoff MJ, Boney-Montoya J, Choi M, et al. FGF15/19 regulates hepatic glucose metabolism by inhibiting the CREB-PGC-1α pathway. Cell Metab 2011;13:729–738

35. Lo Sasso G, Murzilli S, Salvatore L, et al. Intestinal specific LXR activation stimulates reverse cholesterol transport and protects from atherosclerosis. Cell Metab 2010;12:187–193

36. Duval C, Touche V, Tailleux A, et al. Niemann-Pick C1 like 1 gene expression is down-regulated by LXR activators in the intestine. Biochem Biophys Res Commun 2006;340:1259–1263

37. Iqbal J, Hussain MM. Intestinal lipid absorption. Am J Physiol Endocrinol Metab 2009;296:E1183–E1194

38. Stahl A, Hirsch DJ, Gimeno RE, et al. Identification of the major intestinal fatty acid transport protein. Mol Cell 1999;4:299–308

39. Brolin RE. Bariatric surgery and long-term control of morbid obesity. JAMA 2002;288:2793–2796

40. Steinbrook R. Surgery for severe obesity. N Engl J Med 2004;350:1075–1079

41. Buchwald H, Avidor Y, Braunwald E, et al. Bariatric surgery: a systematic review and meta-analysis. JAMA 2004;292:1724–1737

42. Thaler JP, Cummings DE. Minireview: hormonal and metabolic mechanisms of diabetes remission after gastrointestinal surgery. Endocrinology 2009;150:2518–2525

43. Wickremesekera K, Miller G, Naotunne TD, Knowles G, Stubbs RS. Loss of insulin resistance after Roux-en-Y gastric bypass surgery: a time course study. Obes Surg 2005;15:474–481

44. Schauer PR, Burguera B, Ikramuddin S, et al. Effect of laparoscopic Roux-en Y gastric bypass on type 2 diabetes mellitus. Ann Surg 2003;238:467–484; discussion 84–85

45. Clements RH, Gonzalez QH, Long CI, Wittert G, Laws HL. Hormonal changes after Roux-en Y gastric bypass for morbid obesity and the control of type-II diabetes mellitus. Am Surg 2004;70:1–4; discussion 4–5

46. Strader AD. Ileal transposition provides insight into the effectiveness of gastric bypass surgery. Physiol Behav 2006;88:277–282

47. Rodieux F, Giusti V, D'Alessio DA, Suter M, Tappy L. Effects of gastric bypass and gastric banding on glucose kinetics and gut hormone release. Obesity (Silver Spring) 2008;16:298–305

48. Wu AL, Coulter S, Liddle C, et al. FGF19 regulates cell proliferation, glucose and bile acid metabolism via FGFR4-dependent and independent pathways. PLoS ONE 2011;6:e17868

49. Kong B, Wang L, Chiang JY, Zhang Y, Klaassen CD, Guo GL. Mechanism of tissue-specific farnesoid X receptor in suppressing the expression of genes in bile-acid synthesis in mice. Hepatology 2012;56:1034–1043

50. Kir S, Beddow SA, Samuel VT, et al. FGF19 as a postprandial, insulin-independent activator of hepatic protein and glycogen synthesis. Science 2011;331:1621–1624